

DOI: 10.1002/adma.200601552

# Single-Electron Transfer in Nanoparticle Solids\*\*

By Sulolit Pradhan, Jia Sun, Fengjun Deng, and Shaowei Chen\*

Monolayer-protected nanoparticles exhibit unique electronic conductivity properties, which can be tailored by the combined effects of the conductive inorganic cores and the insulating organic shells. In scanning tunneling spectroscopic (STS) studies of isolated particles,<sup>[1–3]</sup> the resulting current–potential ( $I$ – $V$ ) profile generally exhibits a Coulomb blockade in the central region, beyond which a Coulomb staircase (single-electron transfer; SET) may be identified. Such unique characteristics are the fundamental basis for the development of single-electron transistors.<sup>[4]</sup> By contrast, in studies of nanoparticle ensembles that form (sub)micrometer-thick solid films,<sup>[5–8]</sup> typically only linear (Ohmic)  $I$ – $V$  behavior is observed, especially at a relatively high voltage bias, because of rampant structural defects within these particle solids that facilitate interparticle charge transfer (e.g., percolation effects). Fundamentally, the collective conductivity properties of organized assemblies of particles are found to be determined not only by the particle chemical structure (core size, shape, and surface ligands), but by the specific chemical environments and interparticle interactions as well.<sup>[9]</sup>

Whereas the electrochemical analogue of the Coulomb-staircase phenomenon has been observed in studies of particles dissolved in an electrolyte solution,<sup>[10]</sup> quantized charge transfer in nanoparticle solids has remained elusive. Thus, an immediate question arises—can single-electron transfer be realized with nanoparticle solids? The fact that nanoparticle solid thin films (monolayers or more complicated organized assemblies) can be readily fabricated by using the Langmuir–Blodgett (LB) or self-assembly technique means that achieving solid-state single-electron transfer will offer a significant advance towards the development of nanoparticle-based single-electron transistors<sup>[4,11]</sup> without the necessity of sophisticated instrumentation (e.g., a scanning tunneling microscope).

Herein we report a recent breakthrough using monolayers of moderately disperse gold nanoparticles, in which well-defined single-electron transfer is observed for the first time in the solid state. Our primary goal here is to identify key param-

eters that are important to realize SET in nanoparticle solid films. As the structural intermediate between isolated particles and thick particle films, particle monolayers exhibit unique electronic conductivity properties. For instance, Heath and co-workers<sup>[12]</sup> observed an insulator–metal transition of a Langmuir monolayer of alkanethiolate-protected silver (AgSR) nanoparticles when the interparticle spacing was sufficiently small. Such a transition was also manifested in electrochemical impedance measurements,<sup>[13]</sup> and in scanning electrochemical microscopy (SECM) studies.<sup>[14,15]</sup> However, in these early studies,<sup>[12–15]</sup> the particle-conductivity profiles did not exhibit the characteristics of quantized charging of the particle molecular capacitance, most probably because the particles used were too big and/or too polydisperse.

In the present study, the gold nanoparticles were protected by a hexanethiolate monolayer (denoted as C6Au), and were synthesized by the Brust protocol.<sup>[16]</sup> The particles then underwent careful fractionation by using a binary solvent–nonsolvent mixture of toluene and ethanol,<sup>[17,18]</sup> and thermal annealing in toluene<sup>[19]</sup> at 110 °C for 8 h in an oil bath in order to reduce the core-size dispersity. The fraction with an average core diameter of 2.0 nm and core-size dispersity of ca. 20 % (as determined by transmission electron microscopy measurements, with the particle composition approximated as Au<sub>314</sub>(C6)<sub>91</sub><sup>[20]</sup>) was used in the subsequent measurements. A monolayer of the C6Au nanoparticles was then deposited by using the LB technique (i.e., vertical deposition) at controlled interparticle separation (calculated by assuming a hexagonal close-packed structure) onto an interdigitated array (IDA) electrode, in order to take conductivity measurements. In a typical experiment, a known amount of the particle solution, typically 1 mg mL<sup>−1</sup> in hexane, was first spread onto the water surface (water resistance > 18 M $\Omega$ , from a Barnstead Nanopure Water System) in an LB trough (NIMA 611D) and at least 30 min was allowed for solvent evaporation before the first compression and between compression cycles. A representative isotherm is included in the Supporting Information (Fig. S1). The particle monolayer was then deposited onto an IDA electrode (25 pairs of gold fingers of dimensions 3 mm  $\times$  5  $\mu$ m  $\times$  5  $\mu$ m, from Abtech) whose surface was coated beforehand by a self-assembled monolayer of butanethiols to render it hydrophobic (the dipper speed was set at 1 mm min<sup>−1</sup>). Once deposition was complete, the IDA electrode with the particle monolayer was kept under vacuum (Cryogenic Equipment; JANIS Co.) overnight for solvent (water) evaporation. Electrochemical measurements were then carried out in vacuo at different temperatures (Lake-shore 331 temperature controller) with an EG&G PARC 283

[\*] Prof. S. Chen, S. Pradhan, Dr. J. Sun, Dr. F. Deng  
Department of Chemistry and Biochemistry, University of California  
1156 High Street, Santa Cruz, CA 95064 (USA)  
E-mail: schen@chemistry.ucsc.edu

[\*\*] This work was supported by a National Science Foundation CAREER Award (CHE-0456130), the Petroleum Research Fund from the American Chemical Society (39729-AC5M), and the University of California at Santa Cruz. Supporting Information is available online from Wiley InterScience or from the author.

potentiostat/galvanostat. The temperature range used for these studies was controlled from 160 to 320 K.

Figure 1 shows the cyclic voltammograms (CVs, A) and differential pulse voltammograms (DPVs, B) of a C6Au monolayer at an interparticle (edge–edge) distance ( $l$ ) of 0.72 nm. Here the measurements were carried out in a vacuum and at varied temperatures. There are at least three aspects that warrant attention. First, when the temperature was controlled at 300 and 320 K, there are at least five pairs of well-defined and evenly spaced voltammetric peaks within the potential range of  $-1.0$  to  $+1.0$  V (panels A and B). These are attributable to the single-electron transfer across the nanoparticle monolayers, which is the first of its kind in nanoparticle solid films, to the best of our knowledge. From the potential spacing (0.27 V), the corresponding particle–particle-coupled capacitance ( $C_{pp}$ ) can be evaluated as 0.59 aF (which essentially reflects the junction capacitance between adjacent particles).

Second, such solid-state quantized charging only occurs within a very small temperature range. At lower temperatures (160 to 280 K), no SET features are observed, and the monolayer conductance diminishes drastically by about four orders of magnitude to only  $10^{-11}$  A (panel C). This abrupt change of voltammetric responses compared to those at ambient temperature (panels A and B) appears to coincide with the phase-transition temperature of the C6Au nanoparticle solids, as demonstrated in differential scanning calorimetry (DSC)

measurements.<sup>[17]</sup> If one assumes linear  $I$ – $V$  behavior (panel C), the electronic conductivity of the particle-monolayer film can be readily estimated from the slope. Panel D depicts the temperature dependence of the particle-film conductance. Here, an Arrhenius behavior can be seen within the temperature range of 220 to 280 K, suggesting a thermal-activation mechanism of interparticle charge transfer, with an activation barrier of ca. 76.7 meV.<sup>[21,22]</sup> At ambient temperatures (panel A, 300–320 K), the voltammetric current also increased with increasing temperatures.

At even lower temperatures (160 to 200 K), the conductivity exhibited only a very weak temperature dependence, indicating that the particle monolayer was highly insulating. These observations suggest that temperature is an important and sensitive variable in the regulation of the interparticle charge-transfer properties, by virtue of the combined effects of thermally induced structural transition of the particle films and thermal activation of interparticle electron hopping (Scheme 1).<sup>[23]</sup> The above results also suggest that solid-state SET only occurs within a very narrow range of temperatures where particle-ensemble structure and interparticle-electron-transfer dynamics are optimized.

The structure of the particle monolayer film was further examined by scanning tunneling microscopy (STM) measurements (Fig. 2), where a particle monolayer was deposited onto a Au (111) substrate surface by the LB technique. It can

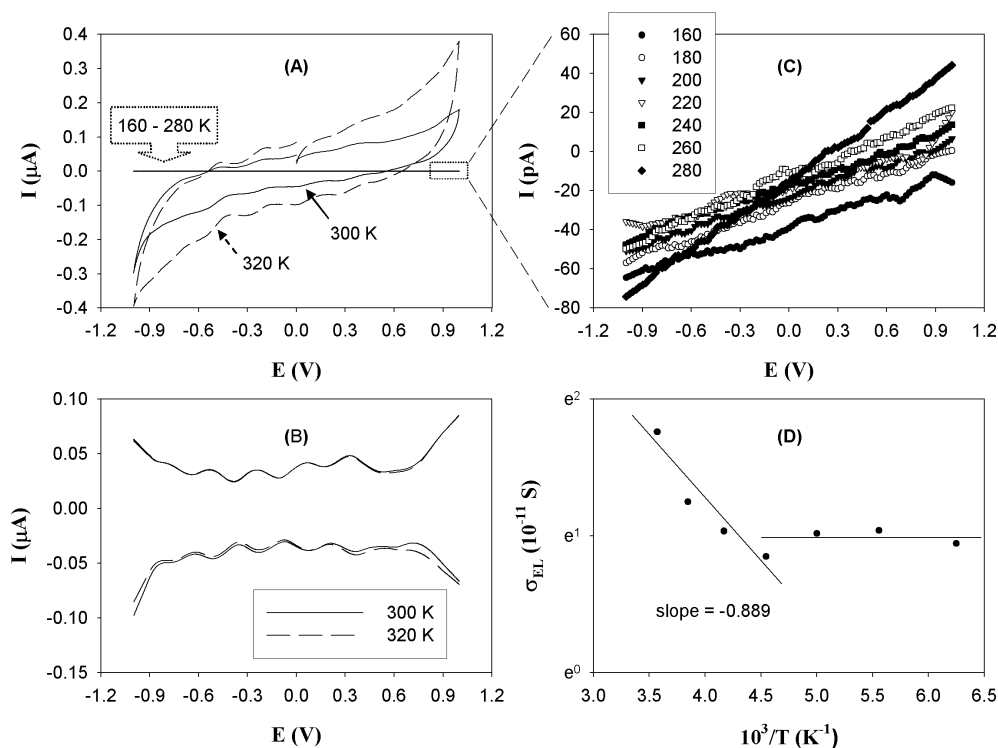
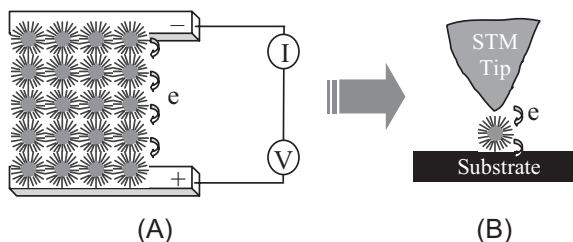


**Figure 1.** A) Cyclic voltammograms of a C6Au nanoparticle monolayer deposited onto an IDA electrode surface by the LB technique at an interparticle edge–edge distance of 0.72 nm. The measurements were carried out in vacuo and at varied temperatures. The potential scan rate was  $20 \text{ mV s}^{-1}$ . B) Differential pulse voltammograms at 300 and 320 K. The pulse amplitude was 50 mV, the pulse width was 200 ms, and the DC ramp was  $20 \text{ mV s}^{-1}$ . C) Amplified CVs of those at 160 to 280 K as shown in (A). D) Semilog plot of the electronic conductivity of the particle monolayers at varied temperatures (160 to 280 K). The symbols show the experimental data collected from the CVs in (C), and the lines show linear regressions.



**Scheme 1.** Schematic of voltammetric studies of nanoparticle monolayers (A) and STM measurements of individual particles (B).

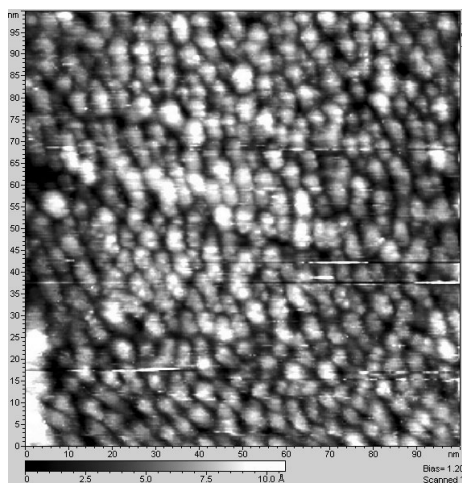


**Figure 2.** STM topographic image of an LB monolayer of C6Au nanoparticles deposited at  $l=0.72$  nm onto a Au (111) substrate surface that was previously coated with a decanethiol self-assembled monolayer. The initial set point was 1.2 V, 20 pA with a PtIr tip. The image was acquired with a Molecular Imaging PicoLE STM/AFM.

be seen that the particles exhibited very good monodispersity and were arranged in a very closely packed structure that falls between a hexagonal distribution and a square lattice.

Third, the interparticle charge-transfer dynamics can be evaluated from the voltammetric measurements. The fact that we observed peaks instead of a staircase (as in STM measurements) can be ascribed to electron diffusion along the particle ensembles. Earlier studies of nanoparticles dispersed in polymer matrices and thick nanoparticle films<sup>[5,24]</sup> have shown that the charge migration (and hence conductance) is essentially limited by electron diffusion within the nanoparticle solids, akin to the case of redox-active polymer melts. Thus, the first-order electron-hopping rate constant ( $k_{ET}$ ,  $s^{-1}$ ) can be calculated from the electron-diffusion coefficient ( $D_{EH}$ ) (assuming a square lattice for the nanoparticle arrays, which is a rather reasonable approximation according to the STM measurements, see below)<sup>[5,24]</sup> to be  $k_{ET}=4D_{EH}/\delta^2$  where  $\delta$  is the interparticle (center-to-center) distance, i.e.,  $\delta=2r+l$ , where  $r$  is the particle radius. Generally, in these nanoparticle solids, physical diffusion of the particles ( $D_{PHYS}$ ) is negligible compared to interparticle electron hopping ( $D_{EH}$ ). Thus, one can approximate  $D_{EH}$  as the overall apparent diffusion coefficient

( $D_{APP}$ ), that is,  $D_{APP}=D_{EH}+D_{PHYS}\approx D_{EH}$ ; the determination of  $D_{APP}$  can be achieved by using sensitive electrochemical techniques. For instance, in differential pulse voltammetry measurements,  $D_{APP}$  can be evaluated from the peak current ( $i_P$ )<sup>[25]</sup>

$$i_P = \frac{nFAD_{APP}^{1/2}C}{(\pi\tau)^{1/2}} \left( \frac{\alpha - 1}{\alpha + 1} \right) \quad (1)$$

where  $n$  is the number of electrons,  $F$  is the Faradaic constant,  $A$  is the electrode surface area,  $C$  is the particle concentration,  $\tau$  is the pulse width, and  $\alpha = \exp(nF\Delta E/2RT)$ , with  $\Delta E$  being the pulse amplitude and  $R$  being the gas constant. At lower temperatures where SET is absent,  $k_{ET}$  can also be evaluated by the ensemble specific conductivity ( $\sigma$ ),<sup>[5]</sup>  $k_{ET}=4RT\sigma/(F^2\delta^2C)$ , where  $T$  is the temperature. Thus, by using these two equations, the interparticle electron-hopping kinetics could be examined within a large range of temperatures, from which further insights into the energetic characteristics and molecular mechanisms could be obtained. For instance, for the C6Au LB monolayer in Figure 1, the electron-hopping rate constant ( $k_{ET}$ ) was found to be of the order of  $10^{10} s^{-1}$  at  $T=300\text{--}320$  K, whereas it decreased drastically to  $10^4 s^{-1}$  when the temperature dropped to 160–280 K.

Similar behavior was also observed with the particle monolayers deposited at different interparticle distances. Figure 3 depicts the  $I$ - $V$  profiles for monolayers of the same C6Au nanoparticles deposited at  $l=0.62$  (Fig. 3A), 1.08 (Fig. 3B), and 1.44 nm (Fig. 3C). It can be seen that at larger interparticle distances, that is,  $l=1.08$  and 1.44 nm, very well defined quantized charging features can also be seen at 290–300 K. The corresponding  $C_{PP}$  can be estimated to be ca. 0.46 aF in both cases, somewhat smaller than that at  $l=0.72$  nm. However, the almost-invariant capacitance at these two longer particle separations seems to imply that the quantized charging currents arose mainly from the particles with very similar interparticle separation in the two latter depositions, most probably because LB deposition is not very effective at large interparticle distances (e.g.,  $l=1.44$  nm, roughly equal to the length of two fully extended hexyl chains), and consequently only closely packed patches of particles were likely to be deposited onto the electrode (considering that the particles are moderately disperse, see above).

At lower temperatures, the current again diminished drastically, akin to what is shown in Figure 1. Additionally, the temperature dependence of the particle conductivity also exhibited an Arrhenius character. Table 1 lists the activation energy for interparticle charge transfer at varied particle spacings, which exhibited a minimum at  $l=0.72\text{--}1.08$  nm, as compared to those at other particle separations or of drop-cast thick films. This minimal activation energy was also coincidental to the occurrence of the SET phenomenon.

By contrast, at smaller interparticle separation ( $l=0.62$  nm, panel A), the  $I$ - $V$  measurements exhibited only featureless re-

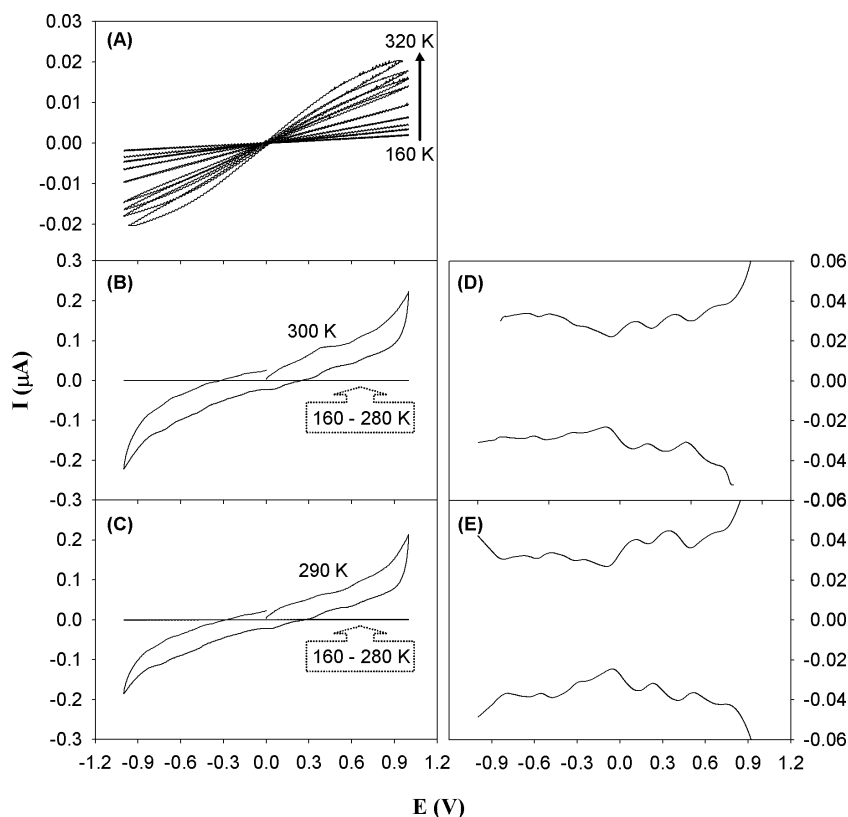


**Figure 3.** Cyclic voltammograms of C6Au monolayers deposited at varied interparticle separations: A) 0.62, B) 1.08, and C) 1.44 nm. For (B) and (C), the corresponding DPVs are shown in (D) and (E), respectively. The experimental temperatures are shown in the individual figure legend: for (A) the data were collected at 160, 190, 220, 250, 280, 290, 300, 310 and 320 K; whereas in (B) and (C), the measurements stopped at 300 and 290 K, respectively. Other experimental conditions are the same as those in Figure 1. To prepare thick particle films, typically the particles were dissolved in toluene at a concentration of 5 mg mL<sup>-1</sup>, and then 5  $\mu$ L was cast onto the IDA electrode surface by using a Hamilton microliter syringe. The particle film was then dried in a gentle nitrogen stream and transferred into the cryogenic vacuum chamber for voltammetric measurements, as detailed above.

**Table 1.** Variation of activation energy ( $E_a$ ) of interparticle charge transfer with interparticle separation ( $l$ ) of LB monolayers of gold nanoparticles.

$l$ [nm]	0.77[a]	0.62	0.72	1.08	1.44
$E_a$ [meV]	225	121	72	71	113

[a] From drop-cast thick films assuming particles are fully intercalated and that the interparticle spacing equals a single ligand length.

sponses where the conductance increased with increasing temperature. Overall, the linear (Ohmic) behavior was very similar to that observed with C6Au drop-cast thick nanoparticle films (Supporting Information, Fig. S2). This seems to imply that at this short interparticle spacing, the enhanced electronic coupling between adjacent particles led to an increase of the particle–particle-coupled capacitance and hence to a diminishment of the quantized charge-transfer character, because in order to observe discrete charge transfer between neighboring particles, the energy barrier for a single-electron transfer ( $e^2/2C_{PP}$ ) must be substantially greater than the thermal kinetic energy ( $k_B T$ , where  $k_B$  is the Boltzmann constant).

From these measurements, one can see that solid-state SET can only be achieved within a narrow range of particle monolayer structures and temperature. It has been found previously that the electronic coupling between neighboring particles and hence the interparticle charge transfer is governed mainly by the ratio ( $\delta/2r$ ) of the particle center-to-center distance ( $\delta$ ) versus the particle-core diameter ( $2r$ ).<sup>[26–28]</sup> For instance, for AgSR particles, at  $\delta/2r > 1.4$ , the ensembles generally behave as Mott insulators, whereas at  $\delta/2r < 1.2$ , a metallic behavior is typically observed. In the above studies (Figs. 1 and 3) where SET is observed, the ratio  $\delta/2r$  is about 1.35 to 1.54. Thus, it is very likely that one major structural condition for SET is that the ratio  $\delta/2r$  should be kept close to the intermediate region between the metal and insulator domains. Coincidentally, using Hamiltonian computation, Remacle<sup>[26]</sup> showed that the Anderson-like transition of the electronic properties of a nanoparticle array occurred at  $\delta/2r \approx 1.3$ .

The above experimental results represent the first observation of SET across a particle solid thin film. In these measurements, the ensemble conductivity is the combined consequence of the interplay of at least three effects:<sup>[27]</sup> i) the disorder from the dispersity of particle-core size, shape, and chemical environments; ii) the dipole coupling between adjacent particles; and iii) the Coulombic repulsion of electrons (of opposite spins) on a given particle. In

these films, disorder within the particle ensembles will diminish the interparticle electronic coupling. Consequently, the electronic wave functions will be localized within individual nanoparticles because of the overwhelming Coulombic barrier to charge migration, leading to low conductivity of the particle solids. The fact that discrete charge transfer can be observed even at moderate electrode potentials indicates that the electronic coupling between the particles should be relatively weak within the present experimental context, and consequently the conductance of the particle monolayer has not reached the “metallic” domain. However, the electronic interactions should be strong enough to overcome the Coulombic barrier and initiate discrete charge transfer between neighboring particles. Consequently, the overall behavior was very similar to those of STM-based measurements of individual nanoparticles (both are in the two-electrode mode, Scheme 1). As the nanoparticle monolayers at the air/water interface can undergo a metal–insulator transition upon mechanical compression,<sup>[12,14]</sup> the present study demonstrated that, with deliberate control of the particle structures and interparticle interactions,

lateral single-electron transfer can also be achieved across these nanoparticle assemblies. This may pave the way toward the development of nanoscale electronic devices (e.g., single-electron transistors) based on organized nanoparticle structures.<sup>[29]</sup>

Received: July 11, 2006

Revised: September 18, 2006

Published online: November 28, 2006

- [1] U. Simon, *Adv. Mater.* **1998**, *10*, 1487.
- [2] D. I. Gittins, D. Bethell, D. J. Schiffrin, R. J. Nichols, *Nature* **2000**, *408*, 67.
- [3] R. P. Andres, T. Bein, M. Dorogi, S. Feng, J. I. Henderson, C. P. Kubiak, W. Mahoney, R. G. Osifchin, R. Reifenberger, *Science* **1996**, *272*, 1323.
- [4] D. L. Feldheim, C. D. Keating, *Chem. Soc. Rev.* **1998**, *27*, 1.
- [5] W. P. Wuelfing, R. W. Murray, *J. Phys. Chem. B* **2002**, *106*, 3139.
- [6] S. D. Evans, S. R. Johnson, Y. L. L. Cheng, T. H. Shen, *J. Mater. Chem.* **2000**, *10*, 183.
- [7] R. C. Doty, H. B. Yu, C. K. Shih, B. A. Korgel, *J. Phys. Chem. B* **2001**, *105*, 8291.
- [8] A. W. Snow, H. Wohltjen, *Chem. Mater.* **1998**, *10*, 947.
- [9] F. Remacle, R. D. Levine, *ChemPhysChem* **2001**, *2*, 20.
- [10] S. W. Chen, R. S. Ingram, M. J. Hostetler, J. J. Pietron, R. W. Murray, T. G. Schaaff, J. T. Khoury, M. M. Alvarez, R. L. Whetten, *Science* **1998**, *280*, 2098.
- [11] K. I. Bolotin, F. Kuemmeth, A. N. Pasupathy, D. C. Ralph, *Appl. Phys. Lett.* **2004**, *84*, 3154.
- [12] G. Markovich, C. P. Collier, S. E. Henrichs, F. Remacle, R. D. Levine, J. R. Heath, *Acc. Chem. Res.* **1999**, *32*, 415.
- [13] G. Markovich, C. P. Collier, J. R. Heath, *Phys. Rev. Lett.* **1998**, *80*, 3807.
- [14] B. M. Quinn, I. Prieto, S. K. Haram, A. J. Bard, *J. Phys. Chem. B* **2001**, *105*, 7474.
- [15] P. Liljeroth, D. Vanmaekelbergh, V. Ruiz, K. Kontturi, H. Jiang, E. Kauppinen, B. M. Quinn, *J. Am. Chem. Soc.* **2004**, *126*, 7126.
- [16] M. Brust, M. Walker, D. Bethell, D. J. Schiffrin, R. Whyman, *J. Chem. Soc. Chem. Commun.* **1994**, 801.
- [17] A. C. Templeton, M. P. Wuelfing, R. W. Murray, *Acc. Chem. Res.* **2000**, *33*, 27.
- [18] R. L. Whetten, M. N. Shafiqullin, J. T. Khoury, T. G. Schaaff, I. Vezmar, M. M. Alvarez, A. Wilkinson, *Acc. Chem. Res.* **1999**, *32*, 397.
- [19] S. W. Chen, *Langmuir* **2001**, *17*, 2878.
- [20] M. J. Hostetler, J. E. Wingate, C. J. Zhong, J. E. Harris, R. W. Vachet, M. R. Clark, J. D. Londono, S. J. Green, J. J. Stokes, G. D. Wignall, G. L. Glish, M. D. Porter, N. D. Evans, R. W. Murray, *Langmuir* **1998**, *14*, 17.
- [21] W. P. Wuelfing, S. J. Green, J. J. Pietron, D. E. Cliffel, R. W. Murray, *J. Am. Chem. Soc.* **2000**, *122*, 11 465.
- [22] M. Brust, D. Bethell, D. J. Schiffrin, C. J. Kiely, *Adv. Mater.* **1995**, *7*, 795.
- [23] T. B. Tran, I. S. Beloborodov, X. M. Lin, T. P. Bigioni, V. M. Vinokur, H. M. Jaeger, *Phys. Rev. Lett.* **2005**, *95*, 076 806.
- [24] J. L. Brennan, M. R. Branham, J. F. Hicks, A. J. Osisek, R. L. Donkers, D. G. Georganopoulou, R. W. Murray, *Anal. Chem.* **2004**, *76*, 5611.
- [25] A. J. Bard, L. R. Faulkner, *Electrochemical Methods: Fundamentals and Applications*, Wiley, New York **2001**.
- [26] F. Remacle, *J. Phys. Chem. A* **2000**, *104*, 4739.
- [27] F. Remacle, R. D. Levine, *J. Am. Chem. Soc.* **2000**, *122*, 4084.
- [28] F. Remacle, K. C. Beverly, J. R. Heath, R. D. Levine, *J. Phys. Chem. B* **2002**, *106*, 4116.
- [29] J. Z. Zhang, Z. L. Wang, J. Liu, S. Chen, G.-Y. Liu, *Self-Assembled Nanostructures*, Kluwer Academic/Plenum Publishers, New York **2003**.